AGU ADVANCING EARTH AND SPACE SCIENCE

Geophysical Research Letters®

RESEARCH LETTER
10.1029/2021GL095933

Conjugate Observation of Magnetospheric Chorus Propagating to the Ionosphere by Ducting

Yangyang Shen[1], Lunjin Chen[2], Xiao-Jia Zhang[1], Anton Artemyev[1,3], Vassilis Angelopoulos[1], Christopher M. Cully[4], H. Gordon James[4], Andrew W. Yau[4], Andrew D. Howarth[4], Jacob Bortnik[5], Jiashu Wu[1], Sheng Tian[6], Michael D. Hartinger[1,7], Martin Connors[8], and Richard B. Horne[9]

[1]Department of Earth, Planetary, and Space Sciences, University of California Los Angeles, Los Angeles, CA, USA, [2]Department of Physics, University of Texas at Dallas, Dallas, TX, USA, [3]Space Research Institute of Russian Academy of Sciences, Moscow, Russia, [4]Department of Physics and Astronomy, University of Calgary, Calgary, AB, Canada, [5]Department of Atmospheric and Oceanic Sciences, University of California, Los Angeles, CA, USA, [6]School of Physics and Astronomy, University of Minnesota, Minneapolis, MN, USA, [7]Space Science Institute, Boulder, CO, USA, [8]Department of Physics and Astronomy, Athabasca University, Calgary, AB, Canada, [9]British Antarctic Survey, Cambridge, UK

Key Points:

- We report first conjugate observations of ducted chorus waves propagating from the equatorial magnetosphere to the ionosphere
- Ducted chorus waves maintain significant wave power upon reaching the ionosphere, which is confirmed by ray-tracing simulations
- Ducted chorus elements bear similar duration and repetition rates to previously reported energetic microbursts

Supporting Information:

Supporting Information may be found in the online version of this article.

Correspondence to:

Y. Shen,
yshen@epss.ucla.edu

Citation:

Shen, Y., Chen, L., Zhang, X.-J., Artemyev, A., Angelopoulos, V., Cully, C. M., et al. (2021). Conjugate observation of magnetospheric chorus propagating to the ionosphere by ducting. *Geophysical Research Letters*, *48*, e2021GL095933. https://doi.org/10.1029/2021GL095933

Received 29 AUG 2021
Accepted 10 NOV 2021

Abstract Whistler-mode chorus waves are critical for driving resonant scattering and loss of radiation belt relativistic electrons into the atmosphere. The resonant energies of electrons scattered by chorus waves increase at increasingly higher magnetic latitudes. Propagation of chorus waves to middle and high latitudes is hampered by wave divergence and Landau damping but is promoted otherwise if ducted by density irregularities. Although ducting theories have been proposed since the 1960s, no conjugate observation of ducted chorus propagation from the equatorial magnetosphere to the ionosphere has been observed so far. Here we provide such an observation, for the first time, using conjugate spacecraft measurements. Ducted chorus waves maintain significant wave power upon reaching the ionosphere, which is confirmed by ray-tracing simulations. Our results suggest that ducted chorus waves may be an important driver for relativistic electron precipitation.

Plain Language Summary We present magnetically conjugate observations of chorus waves propagating from the magnetosphere to the topside ionosphere and subsequently to the ground in ducted mode, that is, guided by density crests as light by optical fibers. In our case event, ducted chorus waves maintain significant wave power upon reaching the ionosphere, which is confirmed by ray-tracing simulations. In addition, ducted chorus elements observed in the ionosphere bear similar timescales and repetition rates (<1 s) to previously reported microburst precipitation. Our observations imply that ducted chorus waves may be an important driver of relativistic electron precipitation from the Earth's radiation belt.

1. Introduction

In the strongly inhomogeneous magnetic field of the Earth, energetic electron scattering and acceleration by chorus waves occurs over a wide range of latitudes for different energies and pitch angles, which makes the latitudinal distribution of chorus wave intensity one of the most important characteristics of wave-particle resonance models in the magnetosphere (Orlova & Shprits, 2010; Summers et al., 2007; Watt et al., 2013). The most intense chorus waves are generated near the geomagnetic equator by anisotropic distributions of hot plasma sheet electrons (Katoh & Omura, 2007; Nunn et al., 2009; Tao, 2014). Decay of wave intensity away from the equatorial source region is dominated by wave divergence (Breuillard et al., 2012; Chum & Santolík, 2005) and Landau damping by suprathermal electron fluxes due to increasingly oblique wave normal vectors in the course of their propagation (Bortnik et al., 2006; Brinca, 1972; Kennel, 1966). This wave decay has been confirmed by statistical spacecraft observations and is pronounced at latitudes greater than ∼20° on the nightside where chorus wave sources are closely confined to near the equator (Meredith et al., 2021).

Although statistical observations have demonstrated much smaller wave power of field-aligned chorus waves and increasing whistler obliquity away from the equatorial source region (Agapitov et al., 2018), a noticeable population of field-aligned lower-band chorus waves were still detected at latitudes beyond 20° and at *L*-shell ∼5–6 (Agapitov et al., 2018; Artemyev et al., 2015; Meredith et al., 2021). Propagation of field-aligned chorus relatively unattenuated to middle and even high latitudes can only be explained by wave ducting through fine-scale plasma density structures, such as crests (Helliwell, 1965; Smith et al., 1960). Such waves are critical for

controlling the balance between scattering loss and acceleration of radiation belt electrons (Mourenas et al., 2014; Thorne, 2010).

Through ray-tracing simulations, previous studies have shown that ducted whistlers propagate without damping and divergence, and sometimes even with significant amplification along convergent field lines (Chen et al., 2017; Hanzelka & Santolík, 2019; Katoh, 2014; Streltsov et al., 2012). In the absence of fine-scale density structures, whistler waves will propagate in a nonducted way, in which they may experience increasingly oblique wave normal angles, followed by magnetospheric reflection and strong Landau damping as the wave frequency approaches the local lower hybrid frequency upon reaching high-latitude regions (Bortnik et al., 2006; Hanzelka & Santolík, 2019; Kimura, 1966). However, both ground-based and magnetospheric observations suggest that whistler waves often experience ducting around the plasmapause (Demekhov et al., 2017; Smith et al., 2010), where strong plasma density gradients or small density irregularities (typically field-aligned) serve as wave guides and channel whistler waves into lower-altitude regions (Inan & Bell, 1977; Woodroffe & Streltsov, 2013). Discrete emissions of whistler waves were observed by spacecraft in the topside ionosphere and have been suggested to originate from the magnetosphere (Bortnik et al., 2007; Santolik et al., 2006). There is also strong evidence of ducted chorus waves in the low-latitude (<20°) magnetosphere (Chen et al., 2021; Ke et al., 2021), and statistics of chorus waves shows a significant population of field-aligned (likely ducted) waves even at middle latitudes (<50°) (Agapitov et al., 2018).

Propagating through the ionosphere, chorus waves are significantly modified via absorption, filtering, and other mechanisms (Bell & Ngo, 1990; Helliwell, 1965; Sonwalkar, 2006), so it is difficult to use ground-based observations to directly infer magnetospheric wave properties. A missing key information is, how much field-aligned chorus wave power can be channeled into resonant interactions with energetic electrons at middle and high latitudes during a given event? Although the statistical distribution of field-aligned chorus wave power up to ∼40° latitude has been provided based on Cluster satellite data (Agapitov et al., 2018; Mourenas et al., 2014; Santolík et al., 2014), no direct evidence of chorus wave ducting and propagation to low altitudes during a particular event has yet been provided. In this paper, we will present the first conjugate observation of ducted chorus waves propagating from the magnetosphere to the ionosphere (∼350 km in altitude) and subsequently being transmitted to the ground. Coordinated observations have been made using data from the Van Allen Probe B (VAP-B) spacecraft (Mauk et al., 2013), the Enhanced Polar Outflow Probe (e-POP) on the CASSIOPE spacecraft (Yau & James, 2015), and the ground-based receiver of the Array for Broadband Observations of VLF/ELF Emissions (ABOVE) (Ghaffari et al., 2020).

2. Data and Observations

From Van Allen Probes, we use measurements from the Electric Field and Waves (EFW) instrument (Wygant et al., 2013) and Electric and Magnetic Field Instrument Suite and Integrated Science (EMFISIS) (Kletzing et al., 2013) which provide electron densities inferred from spacecraft potentials, magnetic and electric field spectra in the frequencies from 10 Hz to 12 kHz, and short-burst (∼6 s) waveform data at 35k samples per second (sps). From e-POP, we use electric field spectra and time series data from the radio receiver instrument (RRI) (James et al., 2015), measuring two-component (in the spacecraft y-z plane excluding the ram x direction) electric fields in the frequency range of ∼7 Hz to 32 kHz with a sampling rate of 62.5k sps in the VLF mode. The ABOVE ground-based VLF receiver (Ghaffari et al., 2020) at Camrose (Canada, L ∼4) measures electromagnetic waves in the frequency range of 100 Hz to 75 kHz.

Figure 1 presents an overview of the chorus waves observed from e-POP, the ABOVE VLF ground-based receiver, and Van Allen Probe B (VAP-B) on 6 November 2014. Figure 1a shows that e-POP (red curve) traveled across the magnetic footprints of $L = 7$ to $L = 4.5$ (where L denotes the distance of the dipole field equatorial crossing from the geomagnetic center in Earth radii) at 2.5 hr magnetic local time (MLT) during the period from 07:29:30 UT to 07:30:40 UT. VAP-B (blue curve) followed 20 min later, traversing neighboring magnetic locations in the inner magnetosphere. e-POP was located at an altitude of 350 km just above the ionospheric density peak, while VAP-B was located near the geomagnetic equator at $L = 5.6$ outside the plasmapause (L ∼5) during the conjunction. Observations of stable and long-lasting (>30 min on VAP-B, and hours by ABOVE on the ground) chorus waves in the same frequency range 0.5–1.5 kHz, where they appear as ducted on VAP-B and e-POP with WNA <30° correlated with density fluctuations, suggest that both e-POP and VAP-B have probably measured

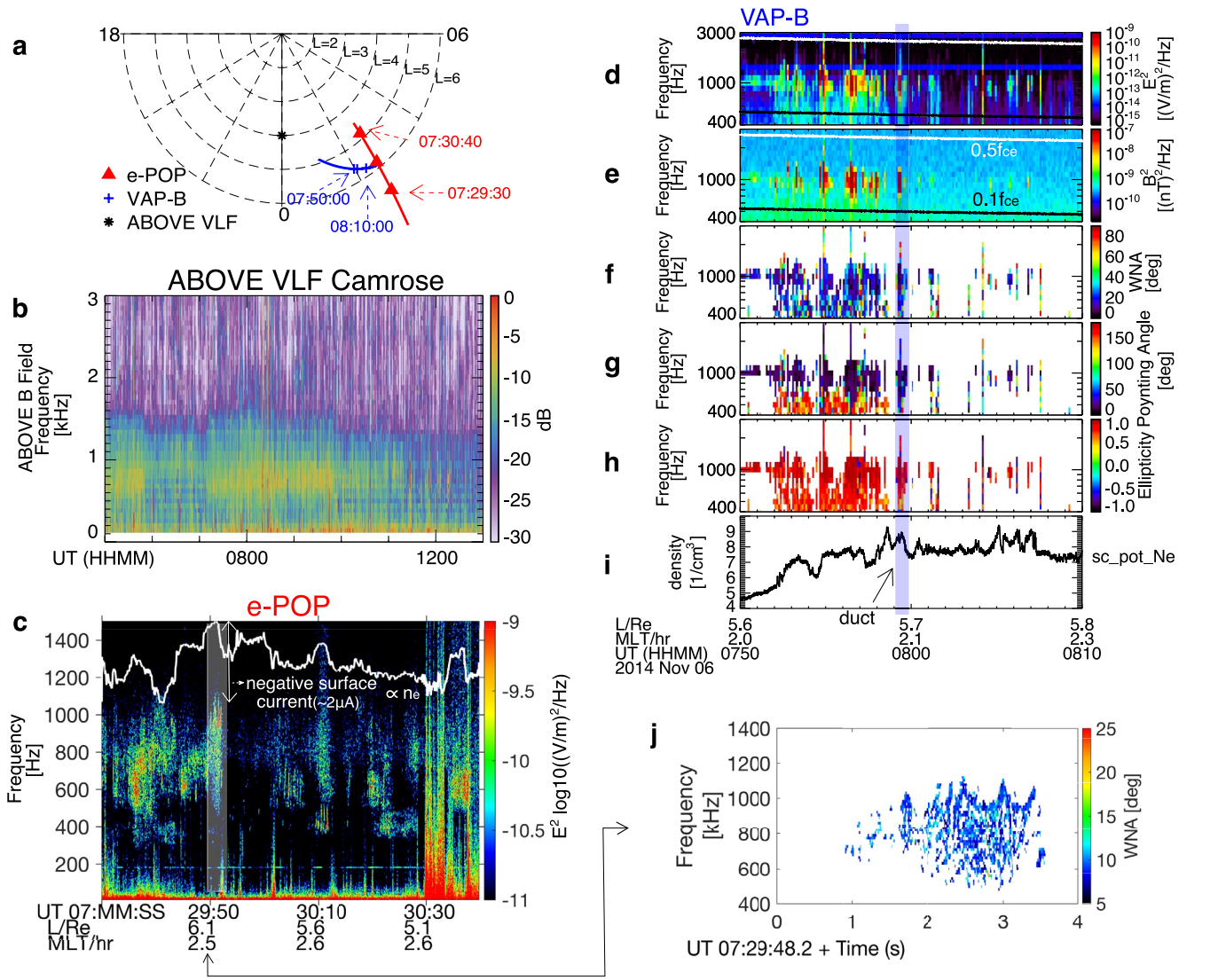

Figure 1. (a) Magnetic footprints of the spacecraft and ground-based receiver in *L*-shell and magnetic local time (MLT). (b) Wave magnetic fields frequency-time spectra measured by Array for Broadband Observations of VLF/ELF Emissions (ABOVE) showing discrete chorus waves (0.4–1.5 kHz). (c) Wave electric fields frequency-time spectra measured by Enhanced Polar Outflow Probe (e-POP) showing discrete chorus and hiss emissions (0.4–1.2 kHz). Sensor surface current measurements from the e-POP Imaging and Rapid-Scanning Ion Mass Spectrometer (IRM) instrument are also displayed to indicate density structures associated with whistler waves. (d) Wave electric field spectra observed by Van Allen Probe B (VAP-B). (e) Wave magnetic field spectra. Half and one tenth of the local electron gyrofrequency (f_{ce}) are indicated as the white and black traces, respectively. (f) Wave normal angles showing mostly field-aligned propagation of chorus waves. (g) Poynting flux vector angle with respect to the magnetic field showing additionally that waves propagate down (blue) the field line to the ionosphere. (h) Wave ellipticity showing right-handed circularly polarized waves. (i) Electron density structures inferred from spacecraft potentials. (j) Wave normal angles for one of the e-POP observed chorus burst within the density duct in (c).

ducted chorus waves coming from the same source region (L ~5–6) and generated by the same electron population injected from the plasma sheet. In fact, based on THEMIS observations outside the plasmapause in the premidnight sector (not shown here), such chorus waves have been associated with a set of substorm injections initiated at 06:30 UT and intensified right at 07:20 UT, after which time injection electrons with similar energies persisted nearly 4 hr.

The e-POP radio receiver instrument measured several bursts of discrete whistler emissions within the frequency range of 0.4–1.2 kHz during the conjugacy period in Figure 1c. No chorus wave emissions were observed in the ionosphere at L-shells larger than $L = 6.5$ and smaller than $L = 5.0$, indicative of relatively confined whistler source regions in the magnetosphere. Notably, pronounced discrete whistler wave packets with internal temporal

modulations of approximately 0.5 s can be identified at several frequency bands near L ~6 from 07:29:50 UT to 07:30:30 UT. For example, near 07:29:50 UT as indicated by the gray-shaded box region in Figure 1c, intensified wave bursts with discrete internal structures, which are the signature of chorus, can be observed at frequencies of 0.9–1.1 kHz. These discrete chorus waves gave way to hiss-like wave emissions at lower frequencies of 0.4–0.9 kHz, although discrete internal structures are still noticeable in hiss-like emissions. Discrete whistler emissions were also identified over the frequency range of 0.4–0.8 kHz near 07:30:05 UT and 07:30:10 UT. Chorus and hiss waves measured by e-POP demonstrate strikingly multifaceted structures in frequency, which occur in bursts across L-shells of 5.0–6.5.

More interestingly, the observed chorus waves are mostly associated with increased electron densities inferred from the surface currents measured by e-POP Imaging and Rapid-Scanning Ion Mass Spectrometer (IRM) sensor (Yau et al., 2015) and displayed as the white trace in Figure 1c. The sensor surface current is a proxy for the electron density and proportional to the latter under typical conditions; increased negative currents indicate density enhancements. Figure 1j shows the wave normal angles of chorus and hiss waves within one of the density crest near 07:29:50 UT, calculated as $\theta = \arctan(E_z/\sqrt{2}E_y)$. Small wave normal angles are consistent with ducted whistler waves propagation. Therefore, these discrete chorus waves appear to have been trapped in the corresponding density ducts and may have originated from the overlying magnetosphere. It should be noted that some of the discrete chorus emissions are not correlated with apparent density enhancements, suggesting that these waves may have exited from the density ducts at altitudes higher than 350 km (Bernhardt & Park, 1977).

Chorus waves were also observed on the ground by the ABOVE VLF receiver at Camrose (L ~4) within the frequency range of 0.4–1.5 kHz (Figure 1b). The difference in L-shell between e-POP and ABOVE observations may be explained by cross-L propagation of whistlers in the Earth-ionosphere waveguide once chorus waves exit from the ionospheric density peak (Helliwell, 1965). In the inner magnetosphere, VAP-B was conjugate to e-POP from 07:50:00 UT to 08:10:00 UT and captured ducted chorus waves with similar characteristics to those in the topside ionosphere. The chorus waves observed by VAP-B and e-POP are likely to come from the same source region and same source electron population despite having a 20-min time separation, because very similar chorus waves were detected on the ground for more than 7 hr from 05:00 UT to 12:00 UT (Figure 1b).

Figures 1d–1i demonstrate the chorus wave characteristics and the associated density duct outside the plasmapause (L ~5) observed from VAP-B. Figures 1d–1e display intense chorus wave packets in the frequency range of 0.6–1.5 kHz (~0.1–~0.4 f_{ce}). Weaker whistler waves can also be identified at frequencies below 0.6 kHz. Figures 1f and 1g display the wave normal angle and Poynting flux polar angle (with 0° corresponding to positive downward flux along the background magnetic field), showing that only chorus waves with frequencies above ~0.5 kHz propagate parallel to B and toward the Earth in the northern hemisphere. Lower-frequency waves are antiparallel to B and are not likely to be observed by e-POP. The measurements of wave ellipticity near +1 shown in Figure 1h are consistent with right-handed circularly polarized whistler-mode waves. More importantly, Figure 1i reveals that density enhancements of up to 25% relative to the background are correlated with a number of discrete, intensified chorus wave bursts. This level of density crests is more than enough to trap whistler waves with frequencies near $0.2f_{ce}$ and wave normal angles less than ~40° as observed in our case (Helliwell, 1965; Smith et al., 1960). These ducted chorus waves will propagate toward the ionosphere and can be detected by e-POP.

3. Comparison of Chorus Wave Electric Field Time Series and Spectra

To further highlight the link between, and variations of chorus waves observed by VAP-B in the magnetosphere and by e-POP in the ionosphere, we examine in detail the chorus wave spectra and waveform packets. Figure 2 demonstrates a comparison of frequency spectra and waveform electric fields measured by VAP-B and e-POP during the conjunction. We have identified a number of characteristic spectra of discrete whistler bursts with large amplitudes and compare them in Figures 2a and 2b. Although the wave power of chorus measured by VAP-B is mostly concentrated in the frequency band of 0.7–1.5 kHz, with a distinct spectral peak at near 1 kHz exceeding 10^{-3} $(\mathrm{mV/m})^2/\mathrm{Hz}$, the whistler wave intensity measured by e-POP extends to lower frequencies covering 0.4–1.0 kHz, with slightly smaller peaks at several frequencies approaching 10^{-3} $(\mathrm{mV/m})^2/\mathrm{Hz}$. Overall, chorus waves preserve significant (at least more than 10%) wave power as they are channeled from the magnetosphere

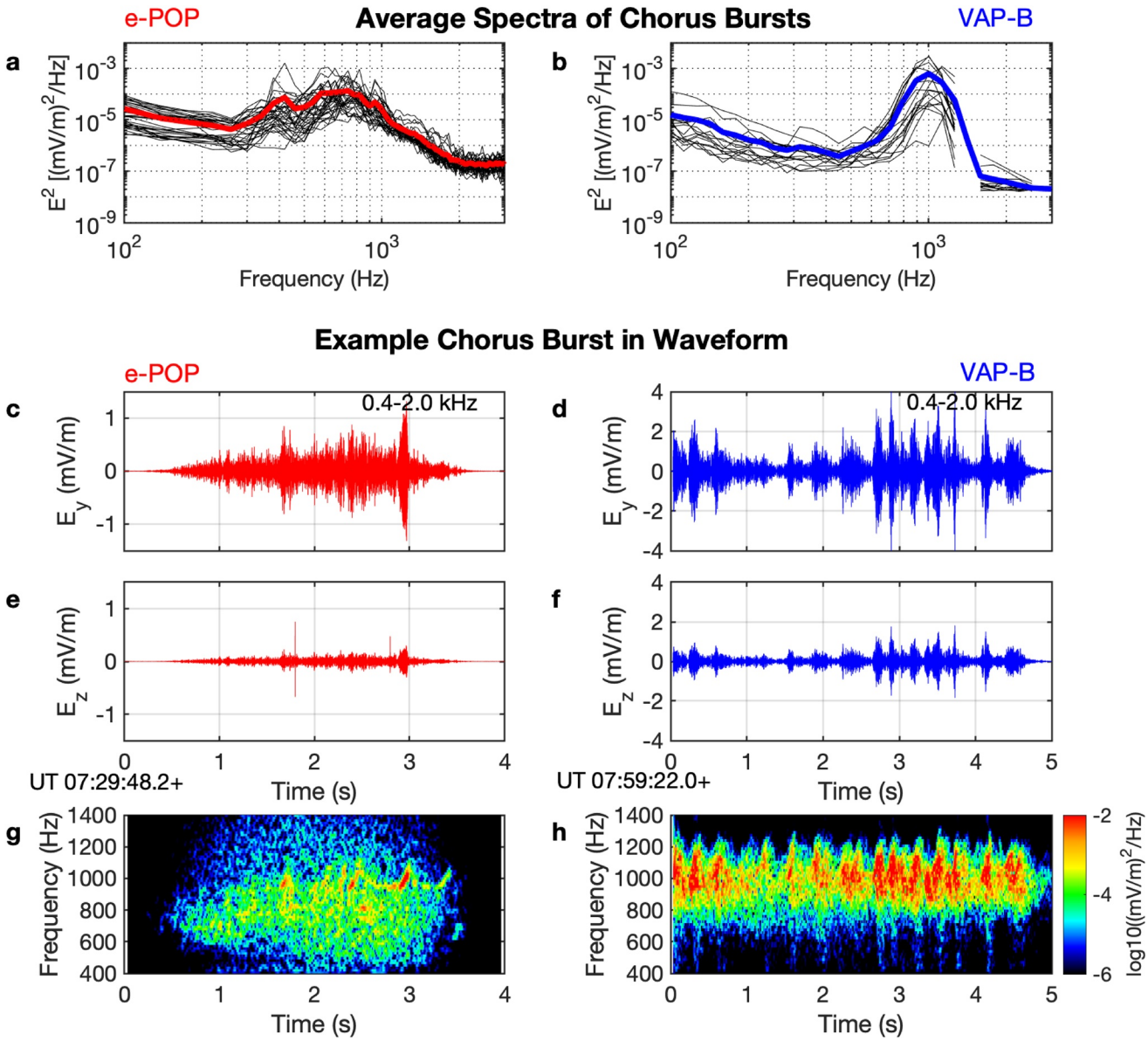

Figure 2. (a) Thirty-four characteristic spectra of chorus wave packets, selected when Enhanced Polar Outflow Probe (e-POP) observed pronounced discrete whistler emissions as shown in Figure 1b. Each spectrum is calculated from 0.5-s waveforms, to match with Van Allen Probe B (VAP-B) spectra measurements. The mean values of the spectra are displayed as the red curve. (b) Sixteen characteristic spectra of chorus wave packets, selected when VAP-B observed pronounced discrete whistler emissions as shown in Figure 1d. VAP-B survey spectra data are generated from ~0.5 s waveforms every 6 s. The blue curve displays their mean spectrum. (c), (e) 4-s waveform electric fields (spacecraft *y* and *z* components) of one chorus wave burst measured by e-POP as highlighted by the gray-shaded box in Figure 1b. (d), (f) 5-s waveform electric fields (*y* (perpendicular) and *z* (parallel) components) of one chorus wave packet measured by VAP-B as highlighted by the blue-shaded box in Figure 1d. (g) Frequency-time spectrogram of chorus waves measured by e-POP, calculated using perpendicular E_y electric fields in panel (c). (h) Frequency-time spectrogram of chorus wave measured by VAP-B, calculated using perpendicular E_y electric fields measured by VAP-B in panel (d).

into the ionosphere in ducted mode, if we assume the chorus wave activity is relatively stable during the period of conjunction as shown by the ground-based measurement (Figure 1c).

To demonstrate the link between e-POP and VAP observed chorus, we show example waveform measurements of a single chorus burst during the conjunction. The intervals selected for waveform comparison are highlighted by the gray-shaded and blue-shaded rectangular boxes in Figures 1c and 1d. Both electric field time series have been band-pass filtered to the frequencies of 0.4–2.0 kHz. Because the local magnetic field at the e-POP position is only 12° away from the spacecraft coordinates *z* direction, E_y and E_z in Figures 2c and 2e represent approximately the perpendicular and parallel electric field component, respectively. By examining electric field hodograms

containing E_y and E_z, it appears that these waves rotate in the right-handed polarized sense, as expected for whistler-mode waves.

Markedly, the waveform electric fields measured by VAP-B and e-POP both display internal structures with a period of ∼0.3 s. These fine structures can be clearly identified in Figures 2g and 2h, in which Fourier frequency-time spectra of chorus waves demonstrate typical characteristics of mostly rising-tone but occasionally falling-tone elements in the frequencies of ∼0.7–1.2 kHz. More importantly, several rising-tone elements near 1 kHz detected by e-POP in the ionosphere have wave power of up to 10^{-2} $(mV/m)^2/Hz$, comparable with that measured by VAP-B in the magnetosphere.

Despite similar rising and falling tones, chorus waves measured by e-POP are generally less intense, less coherent, and narrower in bandwidth than their counterparts measured by VAP-B, as shown in Figures 2g and 2h. In addition to chorus elements, the ducted whistler packets measured by e-POP have significant hiss-like wave power at frequencies below 0.8 kHz, which differs from the VAP-B observation. These hiss-like unstructured emissions may have been generated by discrete chorus emissions during their dispersive propagation toward the ionosphere (Bortnik et al., 2008, 2009; Li et al., 2015). Escaping from a duct may also contribute to the loss of coherency during the propagation. A slight difference in wave normal angles of chorus and hiss waves is discernible in Figure 1j.

4. Whistler Ray-Tracing Simulations

To verify our hypothesis that the chorus waves observed by e-POP in the ionosphere are causally related to equatorial chorus waves similar to the waves simultaneously measured by VAP-B in the magnetosphere at a nearby *L*-shell and MLT, we use 2D (in the meridional plane) HOTRAY (Bortnik et al., 2011; Horne, 1989) ray-tracing simulations to model propagation and evolution of ducted and nonducted chorus from the equatorial magnetosphere to high latitudes. Two-dimensional simulations are justified because the observed conjugate chorus waves are relatively confined in MLT (∼2–3 hr). We have adopted a dipole magnetic field and a diffusive equilibrium cold plasma density model (Bortnik et al., 2011). Electron distributions used for the Landau damping calculation are based on THEMIS statistics of electron measurements over the suprathermal energy range (∼0.1–26 keV), parameterized by *L*-shell, MLT and Planetary *K*-index (*Kp*) (Chen et al., 2013). On top of the cold plasma density model with a plasmapause inner edge at $L = 5$, we superpose a small field-aligned density duct centered at $L = 5.6$, according to VAP-B observations. The density duct is added by introducing an enhancement factor of 20% relative to the background and a spatial Gaussian width of 0.1 *L*. This density increase corresponds to a density enhancement of less than 2 cm^{-3} in spacecraft measurements.

We first specify in the simulation 13 whistler rays, spanning the frequencies of 300–15,00 Hz and initiated with parallel propagation from the equatorial magnetosphere within the duct. Figures 3a1–3f1 display wave propagation characteristics of 13 ducted chorus rays. Although higher-frequency chorus waves propagate with larger group velocities than lower-frequency ones, all of the chorus rays are effectively trapped within the small density crest (of a 20% increase) and reach the ionosphere within approximately 1 s. The chorus waves travel coherently in ducted mode and have quasi-parallel propagation along the field line, albeit with undulation in wave normal angles. This undulation signifies that the rays do not propagate exactly parallel to the field within the duct, but are internally reflected into the duct near the edges, similar to guiding of light by optical fibers. The slight deviation from the field-aligned direction leads to a small level of Landau damping; higher-frequency chorus waves experience larger damping (approximately 80% power decay upon reaching the ionosphere for the chorus at 1.5 kHz) than the lower-frequency ones (Figure 3f1). Stronger Landau damping for higher-frequency chorus may partly explain the prevalence of low-frequency (0.4–1.0 kHz) chorus observed by e-POP. Overall, at frequencies below 1 kHz, chorus waves can reach the ionosphere in ducted mode with little wave power decay. The simulated features of quasi-parallel ducted propagation and relatively unattenuated chorus elements reaching the ionosphere are consistent with VAP-B and e-POP observations.

Upon reaching ionospheric altitudes, several high-frequency (>1 kHz) chorus rays escape from the density duct and leak to smaller *L*-shell regions. This leakage is attributed to intertwined density structures, including ionospheric densities, plasmapause densities, and the density duct, when the rays arrive at high latitudes where magnetic field lines converge. This superposition of density structures destroys the balance of the refractive index of the trapped chorus on the two edges of the density duct, leading to irreversible wave leakage. The wave leakage

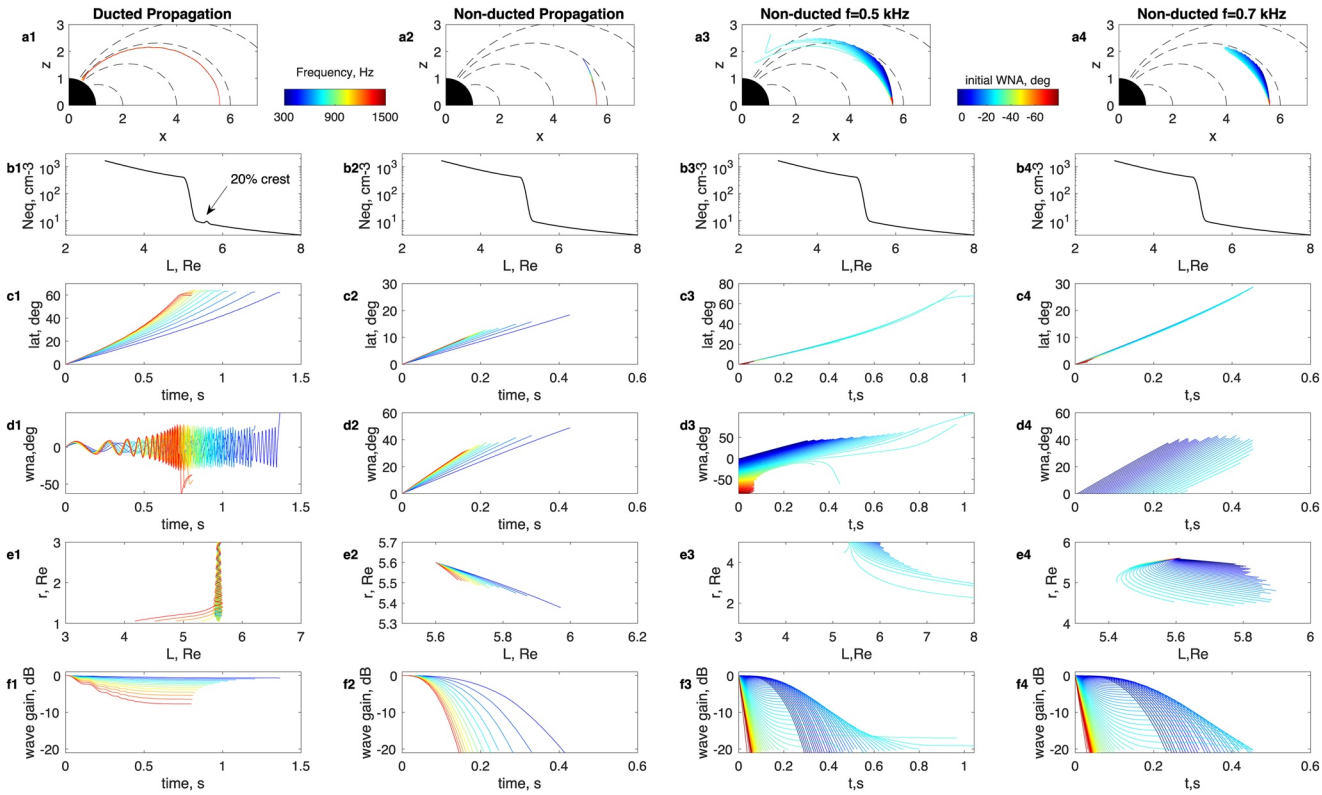

Figure 3. First two columns of panels show ray-tracing simulations of ducted (a1–f1) and nonducted (a2–f2) whistler wave propagation, with 13 individual rays, launched with a field-aligned wave normal angle but different frequencies in the range of 300–1,500 Hz. The third and fourth columns of panels show further nonducted whistler propagation, with 84 rays, launched with a range of initial wave normal angles and a frequency of 0.5 kHz (a3–f3) and 0.7 kHz (a4–f4). The vertical panels from a to f are: whistler ray trajectories in the dipole field x-*z* plane; background density with and without a density duct in *L*; evolution of ray positions in magnetic latitude; evolution of chorus wave normal angles; evolution of chorus ray trajectories in geocentric distance; evolution of chorus rays wave power decay in decibel due to Landau damping. Ray tracing is terminated when reaching below a critical path-integrated gain of −20 dB.

at low altitudes may result in an overlap of chorus wave bursts from different *L*-shells. Furthermore, the leakage may also be responsible for the loss of coherency after propagation over an extended path and account for the observed hiss-like spectra from e-POP.

Without a density duct, however, initially parallel-propagating chorus waves suffer severe Landau damping (Figure 3f2) because their wave normal angles become increasingly oblique to the field line direction (Figure 3d2), a condition favorable to Landau damping (Bortnik et al., 2006; Brinca, 1972; Kennel, 1966). The chorus wave power attenuates to be less than 1% of its original value in less than 0.4 s, with the higher-frequency chorus being damped more rapidly than low-frequency chorus. As a result, no chorus waves can reach high latitudes beyond 20° in Figure 3c2.

To understand whether our event can be related to nonducted whistler propagation, in a way similar to past simulations of hiss wave leaking to the plasmasphere (Bortnik et al., 2011), we also simulate whistler propagation initiated with a range of wave normal angles (Figures 3a3–3a4 and 3a4–3f4) and wave vectors azimuthally facing inward (negative angles). These inward-facing chorus waves will suffer less Landau damping because of the tendency of outward refraction (Bortnik et al., 2011). In Figures 3a3–3f3, only a couple of waves with intermediate wave normal angles can reach the highest latitude of ∼60° (Figure 3c3), but none can reach an altitude below 1,500 km where e-POP is located. Waves with frequencies higher than ∼500 Hz will suffer more damping (Figures 3f3–3f4) and are limited to be within 30° latitude (Figure 3c4). This is consistent with previous simulations showing limited access of chorus waves to high latitudes, particularly with frequencies and at locations relevant to our observations (∼500–1,200 Hz, MLT 2–3 and *L* ∼5.6, Agapitov et al., 2018; Meredith et al., 2021). Comparing ducted and nonducted chorus propagation in Figure 3, we conclude that no significant chorus wave power at >500 Hz can reach low altitudes at the e-POP location without the presence of density ducts. At dayside, with

much less electron Landau damping, nonducted waves can travel to higher latitudes and contribute to plasmaspheric hiss (Bortnik et al., 2011) and low-altitude ionospheric hiss (Xia et al., 2019).

5. Discussion and Conclusion

Although over the last decade, the importance of chorus waves has been recognized in balancing acceleration and loss of radiation belt electrons (Mourenas et al., 2014; Thorne, 2010) and in generating diffuse and pulsating auroras (Kasahara et al., 2018; Thorne et al., 2010) both on Earth and other magnetized planets (Li et al., 2017), the associated wave-particle interaction is often thought to occur primarily near the equator where chorus waves are generated (Katoh & Omura, 2007; Nunn et al., 2009; Tao, 2014). Only when ducted by density irregularities can field-aligned chorus waves propagate to middle and high latitudes (e.g., $>\sim 20°$) without severe attenuation and control wave-particle interaction there (Hanzelka & Santolík, 2019). This ducted propagation to the ionosphere has not yet been observed in a particular event. Using magnetically conjugate chorus observations from e-POP in the ionosphere (~350 km in altitude) and VAP-B in the magnetosphere (L ~5–6) along with ray-tracing simulations to help interpret these observations, we have provided first evidence that lower-band chorus waves generated in Earth's equatorial magnetosphere travel to the ionosphere in ducted mode.

Through ducting which enables chorus to preserve a substantial fraction of its wave power at middle (or even high) latitudes, these off-equator chorus waves will have a critical impact on acceleration and loss of Earth's radiation belt electrons, those with energies from hundreds of keV up to several MeV (Horne & Thorne, 2003; Millan & Thorne, 2007; Summers et al., 1998). Of these, a type of short-lived (<1 s), intense and often relativistic (>500 keV) electron precipitation, known as "microbursts," has been primarily attributed to resonant interactions with chorus waves potentially at middle ($\in [20, 40]°$) latitudes (Breneman et al., 2017; Horne & Thorne, 2003; Imhof et al., 1992; Lorentzen et al., 2000). This microburst precipitation is a major loss process for the outer radiation belt during storms (Lorentzen et al., 2000).

Ducted chorus waves observed by e-POP and VAP-B may be associated with microburst precipitation for several reasons: (a) ducted chorus elements observed in the ionosphere bear similar duration and repetition rates (<1 s) to microbursts; (b) the chorus observations are around the postmidnight sectors (MLT ~2.5) outside the plasmapause (L ~5) where microbursts are often measured (Lorentzen et al., 2000); (c) the observed quasi-parallel chorus waves in the frequency range of 0.4–1.2 kHz can theoretically induce energetic electron precipitation with minimum cyclotron resonant energies from ~100 keV at the magnetic latitude of 10° to greater than 3 MeV at 40° (Horne & Thorne, 2003; Summers et al., 1998) (see also the calculation provided in Figure S1). The estimated minimum resonant energies coincide with the previously observed energetic microbursts (Breneman et al., 2017; Imhof et al., 1992; Lorentzen et al., 2000; Millan & Thorne, 2007; O'Brien et al., 2004).

Finally, the main mechanism suggested for explaining short and intense microburst precipitation is nonlinear resonant electron scattering by chorus waves (Breneman et al., 2017; Chen et al., 2021; Shumko et al., 2018). Such nonlinear resonances require a high wave coherence (Zhang et al., 2020). The most intense precipitation is expected from the chorus wave generation region where waves are highly coherent (e.g., Hikishima et al., 2010) and background field inhomogeneity is sufficiently weak to provide favorable conditions for nonlinear resonances (e.g., Tobita & Omura, 2018), whereas precipitation from middle latitudes (where relativistic electrons resonate with chorus waves) are expected to be weaker due to lower wave intensity (Chen et al., 2020), stronger magnetic field inhomogeneity, and lower wave coherence (Tsurutani et al., 2011). The ducted wave propagation is ideal to keep wave intensity and coherency sufficiently high up to the middle latitudes where relativistic microbursts are likely generated. Conceivably, these ducted chorus waves and the associated wave-particle interaction processes will have profound implications for interpreting measurements of energetic precipitation events in the ionosphere and riometer absorptions on the ground.

Data Availability Statement

The e-POP RRI and IRM data can be publicly accessed through https://epop-data.phys.ucalgary.ca/. The VAP-B EFW and EMFISIS data are publicly available through http://www.space.umn.edu/rbspefw-data/ and https://emfisis.physics.uiowa.edu/data/index. The ABOVE data are publicly available at https://data.phys.ucalgary.ca/sort_by_project/GO-Canada/GO-ABOVE/. The MATLAB code for analyzing e-POP RRI electric fields, for

calculating the minimum cyclotron resonant energies, and for plotting ray-tracing simulation results (and simulation data) are available through http://doi.org/10.5281/zenodo.5576596. The analysis of the Van Allen Probe data is carried out using the standard SPEDAS software package (v4.1) through https://spedas.org/.

Acknowledgments
The authors appreciate the Van Allen Probe EMFISIS team for providing wave electric and magnetic field data. In particular, the authors are grateful to George B Hospodarsky and William S. Kurth for verifying our use of EMFISIS data. L. Chen was supported by NASA Grants 80NSSC19K0282 and 80NSSC21K0728. Y. Shen, X.-J. Zhang, and A. Artemyev were supported by NSF Grant 2026375 and NASA Grant 80NSSC21K0729. The work by the EFW team was conducted under JHU/APL contract 922613 (RBSP-EFW). The authors acknowledge the support for the e-POP mission from the European Space Agency Third-Party Mission Programme, the Canadian Space Agency, and the NSERC Discovery Grants Program (TGPIN-2014-06069). ABOVE is a joint Canada Foundation for Innovation and Canadian Space Agency project developed by the University of Calgary. Operations are supported through the Canadian Space Agency's Geospace Observatory program.

References

Agapitov, O. V., Mourenas, D., Artemyev, A. V., Mozer, F. S., Hospodarsky, G., Bonnell, J., & Krasnoselskikh, V. (2018). Synthetic empirical chorus wave model from combined Van Allen Probes and cluster statistics. *Journal of Geophysical Research: Space Physics*, *123*, 297–314. https://doi.org/10.1002/2017JA024843

Artemyev, A. V., Agapitov, O. V., Mourenas, D., Krasnoselskikh, V. V., & Mozer, F. S. (2015). Wave energy budget analysis in the Earth's radiation belts uncovers a missing energy. *Nature Communications*, *6*, 8143. https://doi.org/10.1038/ncomms8143

Bell, T. F., & Ngo, H. D. (1990). Electrostatic lower hybrid waves excited by electromagnetic whistler mode waves scattering from planar magnetic-field-aligned plasma density irregularities. *Journal of Geophysical Research*, *95*(A1), 149–172. https://doi.org/10.1029/JA095iA01p00149

Bernhardt, P. A., & Park, C. G. (1977). Protonospheric-ionospheric modeling of vlf ducts. *Journal of Geophysical Research*, *82*(32), 5222–5230. https://doi.org/10.1029/JA082i032p05222

Bortnik, J., Chen, L., Li, W., Thorne, R. M., & Horne, R. B. (2011). Modeling the evolution of chorus waves into plasmaspheric hiss. *Journal of Geophysical Research*, *116*, A08221. https://doi.org/10.1029/2011JA016499

Bortnik, J., Inan, U. S., & Bell, T. F. (2006). Landau damping and resultant unidirectional propagation of chorus waves. *Geophysical Research Letters*, *33*, L03102. https://doi.org/10.1029/2005GL024553

Bortnik, J., Li, W., Thorne, R. M., Angelopoulos, V., Cully, C., Bonnell, J., et al. (2009). An observation linking the origin of plasmaspheric hiss to discrete chorus emissions. *Science*, *324*(5928), 775–778. https://doi.org/10.1126/science.1171273

Bortnik, J., Thorne, R. M., & Meredith, N. P. (2008). The unexpected origin of plasmaspheric hiss from discrete chorus emissions. *Nature*, *452*, 62–66. https://doi.org/10.1038/nature06741

Bortnik, J., Thorne, R. M., Meredith, N. P., & Santolik, O. (2007). Ray tracing of penetrating chorus and its implications for the radiation belts. *Geophysical Research Letters*, *34*, L15109. https://doi.org/10.1029/2007GL030040

Breneman, A. W., Crew, A., Sample, J., Klumpar, D., Johnson, A., Agapitov, O., et al. (2017). Observations directly linking relativistic electron microbursts to whistler mode chorus: Van Allen probes and firebird ii. *Geophysical Research Letters*, *44*, 11265–11272. https://doi.org/10.1002/2017GL075001

Breuillard, H., Zaliznyak, Y., Krasnoselskikh, V., Agapitov, O., Artemyev, A., & Rolland, G. (2012). Chorus wave-normal statistics in the Earth's radiation belts from ray tracing technique. *Annales Geophysicae*, *30*, 1223–1233. https://doi.org/10.5194/angeo-30-1223-2012

Brinca, A. L. (1972). On the stability of obliquely propagating whistlers. *Journal of Geophysical Research*, *77*(19), 3495–3507. https://doi.org/10.1029/JA077i019p03495

Chen, L., Breneman, A. W., Xia, Z., & Zhang, X.-J. (2020). Modeling of bouncing electron microbursts induced by ducted chorus waves. *Geophysical Research Letters*, *47*, e2020GL089400. https://doi.org/10.1029/2020GL089400

Chen, L., Santolík, O., Hajoš, M., Zheng, L., Zhima, Z., Heelis, R., et al. (2017). Source of the low-altitude hiss in the ionosphere. *Geophysical Research Letters*, *44*, 2060–2069. https://doi.org/10.1002/2016GL072181

Chen, L., Thorne, R. M., Li, W., & Bortnik, J. (2013). Modeling the wave normal distribution of chorus waves. *Journal of Geophysical Research*, *118*, 1074–1088. https://doi.org/10.1029/2012JA018343

Chen, L., Zhang, X.-J., Artemyev, A., Zheng, L., Xia, Z., Breneman, A. W., & Horne, R. (2021a). Electron microbursts induced by nonducted chorus waves. *Frontiers in Astronomy and Space Sciences*, *8*, 745927. https://doi.org/10.3389/fspas.2021.745927

Chen, R., Gao, X., Lu, Q., Chen, L., Tsurutani, B. T., Li, W., et al. (2021b). In situ observations of whistler-mode chorus waves guided by density ducts. *Journal of Geophysical Research: Space Physics*, *126*, e2020JA028814. https://doi.org/10.1029/2020JA028814

Chum, J., & Santolík, O. (2005). Propagation of whistler-mode chorus to low altitudes: Divergent ray trajectories and ground accessibility. *Annales Geophysicae*, *23*, 3727–3738. https://doi.org/10.5194/angeo-23-3727-2005

Demekhov, A. G., Manninen, J., Santolík, O., & Titova, E. E. (2017). Conjugate ground-spacecraft observations of VLF chorus elements. *Geophysical Research Letters*, *44*, 11735–11744. https://doi.org/10.1002/2017GL076139

Ghaffari, R., Cully, C. M., Turner, D. L., & Reeves, G. D. (2020). Characteristics of electron precipitation during 40 energetic electron injections inferred via subionospheric vlf signal propagation. *Journal of Geophysical Research: Space Physics*, *125*, e2019JA027233. https://doi.org/10.1029/2019JA027233

Hanzelka, M., & Santolík, O. (2019). Effects of ducting on whistler mode chorus or exohiss in the outer radiation belt. *Geophysical Research Letters*, *46*, 5735–5745. https://doi.org/10.1029/2019GL083115

Helliwell, R. A. (1965). *Whistlers and related ionospheric phenomena*. Stanford University Press.

Hikishima, M., Omura, Y., & Summers, D. (2010). Microburst precipitation of energetic electrons associated with chorus wave generation. *Geophysical Research Letters*, *37*, L07103. https://doi.org/10.1029/2010GL042678

Horne, R. B. (1989). Path-integrated growth of electrostatic waves—The generation of terrestrial myriametric radiation. *Journal of Geophysical Research*, *94*(A7), 8895–8909. https://doi.org/10.1029/JA094iA07p08895

Horne, R. B., & Thorne, R. M. (2003). Relativistic electron acceleration and precipitation during resonant interactions with whistler-mode chorus. *Geophysical Research Letters*, *30*(10), 1527. https://doi.org/10.1029/2003GL016973

Imhof, W. L., Voss, H. D., Mobilia, J., Datlowe, D. W., Gaines, E. E., McGlennon, J. P., & Inan, U. S. (1992). Relativistic electron microbursts. *Journal of Geophysical Research*, *97*(A9), 13829–13837. https://doi.org/10.1029/92JA01138

Inan, U. S., & Bell, T. F. (1977). The plasmapause as a VLF wave guide. *Journal of Geophysical Research*, *82*(19), 2819–2827. https://doi.org/10.1029/JA082i019p02819

James, H. G., King, E. P., White, A., Hum, R. H., Lunscher, W., & Siefring, C. L. (2015). The e-POP radio receiver instrument on CASSIOPE. *Space Science Reviews*, *189*, 79–105. https://doi.org/10.1007/s11214-014-0130-y

Kasahara, S., Miyoshi, Y., Yokota, S., Kasahara, Y., Matsuda, S., Kumamoto, A., et al. (2018). Pulsating aurora from electron scattering by chorus waves. *Nature*, *554*, 337–340. https://doi.org/10.1038/nature25505

Katoh, Y. (2014). A simulation study of the propagation of whistler-mode chorus in the Earth's inner magnetosphere. *Earth Planets and Space*, *66*, 6. https://doi.org/10.1186/1880-5981-66-6

Katoh, Y., & Omura, Y. (2007). Computer simulation of chorus wave generation in the Earth's inner magnetosphere. *Geophysical Research Letters*, *34*, L03102. https://doi.org/10.1029/2006GL028594

Ke, Y., Chen, L., Gao, X., Lu, Q., Wang, X., Chen, R., et al. (2021). Whistler-mode waves trapped by density irregularities in the earth's magnetosphere. *Geophysical Research Letters*, *48*, e2020GL092305. https://doi.org/10.1029/2020GL092305

Kennel, C. (1966). Low-frequency whistler mode. *Physics of Fluids*, *9*, 2190–2202. https://doi.org/10.1063/1.1761588

Kimura, I. (1966). Effects of ions on whistler-mode ray tracing. *Radio Science*, *1*(3), 269–284. https://doi.org/10.1002/rds196613269

Kletzing, C. A., Kurth, W. S., Acuna, M., MacDowall, R. J., Torbert, R. B., Averkamp, T., et al. (2013). The electric and magnetic field instrument suite and integrated science (EMFISIS) on RBSP. *Space Science Reviews*, *179*, 127–181. https://doi.org/10.1007/s11214-013-9993-6

Li, W., Chen, L., Bortnik, J., Thorne, R. M., Angelopoulos, V., Kletzing, C. A., et al. (2015). First evidence for chorus at a large geocentric distance as a source of plasmaspheric hiss: Coordinated Themis and Van Allen probes observation. *Geophysical Research Letters*, *42*, 241–248. https://doi.org/10.1002/2014GL062832

Li, W., Thorne, R. M., Ma, Q., Zhang, X.-J., Gladstone, G. R., Hue, V., et al. (2017). Understanding the origin of Jupiter's diffuse aurora using Juno's first perijove observations. *Geophysical Research Letters*, *44*, 10162–10170. https://doi.org/10.1002/2017GL075545

Lorentzen, K. R., McCarthy, M. P., Parks, G. K., Foat, J. E., Millan, R. M., Smith, D. M., et al. (2000). Precipitation of relativistic electrons by interaction with electromagnetic ion cyclotron waves. *Journal of Geophysical Research*, *105*, 5381–5389. https://doi.org/10.1029/1999JA000283

Mauk, B. H., Fox, N. J., Kanekal, S. G., Kessel, R. L., Sibeck, D. G., & Ukhorskiy, A. (2013). Science objectives and rationale for the radiation belt storm probes mission. *Space Science Reviews*, *179*, 3–27. https://doi.org/10.1007/s11214-012-9908-y

Meredith, N. P., Bortnik, J., Horne, R. B., Li, W., & Shen, X.-C. (2021). Statistical investigation of the frequency dependence of the chorus source mechanism of plasmaspheric hiss. *Geophysical Research Letters*, *48*, e2021GL092725. https://doi.org/10.1029/2021GL092725

Millan, R. M., & Thorne, R. M. (2007). Review of radiation belt relativistic electron losses. *Journal of Atmospheric and Solar-Terrestrial Physics*, *69*, 362–377. https://doi.org/10.1016/j.jastp.2006.06.019

Mourenas, D., Artemyev, A. V., Agapitov, O. V., & Krasnoselskikh, V. (2014). Consequences of geomagnetic activity on energization and loss of radiation belt electrons by oblique chorus waves. *Journal of Geophysical Research*, *119*, 2775–2796. https://doi.org/10.1002/2013JA019674

Nunn, D., Santolik, O., Rycroft, M., & Trakhtengerts, V. (2009). On the numerical modelling of VLF chorus dynamical spectra. *Annales Geophysicae*, *27*, 2341–2359. https://doi.org/10.5194/angeo-27-2341-2009

O'Brien, T. P., Looper, M. D., & Blake, J. B. (2004). Quantification of relativistic electron microburst losses during the gem storms. *Geophysical Research Letters*, *31*, L04802. https://doi.org/10.1029/2003GL018621

Orlova, K. G., & Shprits, Y. Y. (2010). Dependence of pitch-angle scattering rates and loss timescales on the magnetic field model. *Geophysical Research Letters*, *37*, L05105. https://doi.org/10.1029/2009GL041639

Santolik, O., Chum, J., Parrot, M., Gurnett, D. A., Pickett, J. S., & Cornilleau-Wehrlin, N. (2006). Propagation of whistler mode chorus to low altitudes: Spacecraft observations of structured elf hiss. *Journal of Geophysical Research*, *111*, A10208. https://doi.org/10.1029/2005JA011462

Santolík, O., Macúšová, E., Kolmašová, I., Cornilleau-Wehrlin, N., & Conchy, Y. (2014). Propagation of lower-band whistler-mode waves in the outer Van Allen belt: Systematic analysis of 11 years of multi-component data from the Cluster spacecraft. *Geophysical Research Letters*, *41*, 2729–2737. https://doi.org/10.1002/2014GL059815

Shumko, M., Turner, D. L., O'Brien, T. P., Claudepierre, S. G., Sample, J., Hartley, D. P., et al. (2018). Evidence of microbursts observed near the equatorial plane in the outer Van Allen radiation belt. *Geophysical Research Letters*, *45*, 8044–8053. https://doi.org/10.1029/2018GL078451

Smith, A., Horne, R., & Meredith, N. (2010). The statistics of natural elf/vlf waves derived from a long continuous set of ground-based observations at high latitude. *Journal of Atmospheric and Solar-Terrestrial Physics*, *72*(5), 463–475. https://doi.org/10.1016/j.jastp.2009.12.018

Smith, R. L., Helliwell, R. A., & Yabroff, I. W. (1960). A theory of trapping of whistlers in field-aligned columns of enhanced ionization. *Journal of Geophysical Research*, *65*(3), 815–823. https://doi.org/10.1029/JZ065i003p00815

Sonwalkar, V. (2006). The influence of plasma density irregularities on whistler-mode wave propagation. In J. W. LaBelle, & R. A. Treumann (Eds.), *Geospace electromagnetic waves and radiation* (pp. 141–190). Springer. https://doi.org/10.1007/3-540-33203-0_6

Streltsov, A. V., Woodroffe, J., Gekelman, W., & Pribyl, P. (2012). Modeling the propagation of whistler-mode waves in the presence of field-aligned density irregularities. *Physics of Plasmas*, *19*(5), 052104. https://doi.org/10.1063/1.4719710

Summers, D., Ni, B., & Meredith, N. P. (2007). Timescales for radiation belt electron acceleration and loss due to resonant wave-particle interactions: 2. Evaluation for VLF chorus, ELF hiss, and electromagnetic ion cyclotron waves. *Journal of Geophysical Research*, *112*, A04207. https://doi.org/10.1029/2006JA011993

Summers, D., Thorne, R. M., & Xiao, F. (1998). Relativistic theory of wave-particle resonant diffusion with application to electron acceleration in the magnetosphere. *Journal of Geophysical Research*, *103*(A9), 20487–20500. https://doi.org/10.1029/98JA01740

Tao, X. (2014). A numerical study of chorus generation and the related variation of wave intensity using the DAWN code. *Journal of Geophysical Research*, *119*, 3362–3372. https://doi.org/10.1002/2014JA019820

Thorne, R. M. (2010). Radiation belt dynamics: The importance of wave-particle interactions. *Geophysical Research Letters*, *372*, L22107. https://doi.org/10.1029/2010GL044990

Thorne, R. M., Ni, B., Tao, X., Horne, R. B., & Meredith, N. P. (2010). Scattering by chorus waves as the dominant cause of diffuse auroral precipitation. *Nature*, *467*, 943–946. https://doi.org/10.1038/nature09467

Tobita, M., & Omura, Y. (2018). Nonlinear dynamics of resonant electrons interacting with coherent Langmuir waves. *Physics of Plasmas*, *25*(3), 032105. https://doi.org/10.1063/1.5018084

Tsurutani, B. T., Falkowski, B. J., Verkhoglyadova, O. P., Pickett, J. S., Santolík, O., & Lakhina, G. S. (2011). Quasi-coherent chorus properties: 1. Implications for wave-particle interactions. *Journal of Geophysical Research*, *116*, A09210. https://doi.org/10.1029/2010JA016237

Watt, C. E. J., Degeling, A. W., & Rankin, R. (2013). Constructing the frequency and wave normal distribution of whistler-mode wave power. *Journal of Geophysical Research*, *118*, 1984–1991. https://doi.org/10.1002/jgra.50231

Woodroffe, J. R., & Streltsov, A. V. (2013). Whistler propagation in the plasmapause. *Journal of Geophysical Research*, *118*, 716–723. https://doi.org/10.1002/jgra.50135

Wygant, J. R., Bonnell, J. W., Goetz, K., Ergun, R. E., Mozer, F. S., Bale, S. D., et al. (2013). The electric field and waves instruments on the radiation belt storm probes mission. *Space Science Reviews*, *179*, 183–220. https://doi.org/10.1007/s11214-013-0013-7

Xia, Z., Chen, L., Zhima, Z., Santolík, O., Horne, R. B., & Parrot, M. (2019). Statistical characteristics of ionospheric hiss waves. *Geophysical Research Letters*, *46*, 7147–7156. https://doi.org/10.1029/2019GL083275

Yau, A., Howarth, A., White, A., Enno, G., & Amerl, P. (2015). Imaging and rapid-scanning ion mass spectrometer (IRM) for the CASSIOPE e-POP mission. *Space Science Reviews*, *189*, 41–63. https://doi.org/10.1007/s11214-015-0149-8

Yau, A. W., & James, H. G. (2015). CASSIOPE enhanced polar outflow probe (e-POP) mission overview. *Space Science Reviews*, *189*(1–4), 3–14. https://doi.org/10.1007/s11214-015-0135-1

Zhang, X.-J., Agapitov, O., Artemyev, A. V., Mourenas, D., Angelopoulos, V., Kurth, W. S., et al. (2020). Phase decoherence within intense chorus wave packets constrains the efficiency of nonlinear resonant electron acceleration. *Geophysical Research Letters*, *47*, e2020GL089807. https://doi.org/10.1029/2020GL089807